TISSUE ENGINEERING: Part A
Volume 17, Numbers 5 and 6, 2011

DOI: 10.1089/ten.tea.2010.0196

In vitro Biomimetic Construction of Hydroxyapatite–Porcine Acellular Dermal Matrix Composite Scaffold for MC3T3-E1 Preosteoblast Culture

Hongshi Zhao, M.Sc.,[1] Guancong Wang, B.Sc.,[1] Shunpeng Hu, M.Sc.,[2] Jingjie Cui, Ph.D.,[1] Na Ren, B.Sc.,[1] Duo Liu, Ph.D.,[1] Hong Liu, Ph.D.,[1] Chengbo Cao, Ph.D.,[2] Jiyang Wang, Ph.D.,[1] and Zhonglin Wang, Ph.D.[3]

The application of porous hydroxyapatite–collagen (HAp-Collagen) as a bone tissue engineering scaffold is hindered by two main problems: its high cost and low initial strength. As a native 3-dimenssional collagen framework, purified porcine acellular dermal matrix (PADM) has been successfully used as a skin tissue engineering scaffold. Here we report its application as a matrix for the preparation of HAp to produce a bone tissue scaffold through a biomimetic chemical process. The HAp-PADM scaffold has two-level pore structure, with large channels ($\sim 100\,\mu m$ in diameter) inherited from the purified PADM microstructure and small pores ($<100\,nm$ in diameter) formed by self-assembled HAp on the channel surfaces. The obtained HAp-PADM scaffold (S15D) has a compressive elastic modulus as high as 600 kPa. The presence of HAp in sample S15D reduces the degradation rate of PADM in collagenase solution at 37°C. After 7 day culture of MC3T3-E1 pre-osteroblasts, MTT data show no statistically significant difference on pure PADM framework and HAp-PADM scaffold ($p > 0.05$). Because of its high strength and nontoxicity, its simple preparation method, and designable and tailorable properties, the HAp-PADM scaffold is expected to have great potential applications in medical treatment of bone defects.

Introduction

Currently, there are increasingly urgent demands for various biomedical bone implants to repair bone defects/damages caused by bone fractures, osteoarthritis, osteoporosis, or bone cancers.[1] However, conventional tissue replacements, such as autografts and allografts, cannot meet the quantity and performance needed by the patients.[2] A large number of 3-dimensional (3D) porous scaffolds have been developed to overcome traditional limitations and have been applied to repair bone defects.[3–5] However, there are still many problems that need to be resolved to meet clinical requirements. Bone is a complex tissue mainly composed of nonstoichiometric hydroxyapatite [$Ca_{10}(PO_4)_6(OH)_2$, HAp] and collagen. Approximately 30–35(wt)% of dry bone is of organic materials, ~95% of which is type I collagen.[6] Collagen, the main organic component of the extracellular matrix (ECM), induces positive effects on cellular attachment, proliferation, and differentiation of many cell types in culture. It has been widely used as a skin substitute material.[7–12] As the main inorganic component of bone, HAp has been widely used in many orthopedic and dental implant materials because of its bioactive,[13–15] osteoconductive, and osteoinductive properties.[16,17] However, pure HAp and collagen cannot be directly used as bone substitute materials, because pure bulk HAp cannot provide a porous structure with biodegradable properties. In addition, a pure collagen framework lacks calcium and has weak initial compressive strength. Therefore, much attention is focused on porous composites of HAp and biodegradable polymers, such as, polylactic acid, gelatin, and chitosan. Compared with other HAp-biodegradable polymer composites, nano-HAp/collagen composites have been approved as a bioactive and biodegradable scaffold due to their chemical and structural similarity to native bone.[18–20]

Normally, HAp-collagen composite bone scaffolds are prepared by two methods: one involves precipitated HAp or *in situ* synthesized HAp nanoparticles that are mixed with a purified collagen solution, followed by cross-linkage and a lyophilization process to develop a porous HAp-collagen composite scaffold.[13,21,22] The other method involves a porous collagen material obtained through the cross-linking of

[1]State Key Laboratory of Crystal Materials, Center of Bio and Micro/Nano Functional Materials, School of Physics and Microelectronics, Shandong University, Jinan, P.R. China.
[2]School of Chemistry and Chemical Engineering, Shandong University, Jinan, China.
[3]School of Materials Science and Engineering, Georgia Institute of Technology, Atlanta, Georgia.

purified collagen in solution and a lyophilization technique, where a layer of HAp nanostructure is then coated by co-precipitation or mineralization.[23–25] Method 1 can provide accurate quantity of the HAp content in the scaffold, whereas method 2 can achieve controlled growth of HAp on collagen. However, both methods are related to soluble pure collagen type I, which is mainly obtained from rat-tail tendon, bovine tendon, or skin.[22,26] The collagen source is very limited, and the extraction process is costly. In addition, the native physiochemical structure of collagen fibrils is likely to be destroyed during the acidic-extraction treatment. When purified collagen is used for the scaffold, it must be re-crosslinked to reconstruct a 3D structure, which increases work load and expense. In addition, glutaraldehyde, which is widely used as cross-linker to prepare the collagen scaffold due to its abundant content, low price, and high crosslinking effect for collagenous tissues, probably causes toxicity when it is released into the host due to biodegradation.[27–29] Moreover, it is very difficult to simulate the natural 3D collagen structure through *in vitro* reconstruction methods. Therefore, there is urgent need in bone tissue engineering to build a very strong 3D collagen framework or selecting a suitable natural collagen framework for the preparation of HAp-collagen composite scaffolds.

Currently, porcine acellular dermal matrix (PADM), which is mainly composed of type I and II collagen has drawn the attention of researchers in many fields due to its excellent achievements in a variety of biomedical applications.[30–33] It has been successfully used in covering full-thickness burn wounds in clinical practice.[34,35] At present, the extraction and purification of ADM from porcine skin has become a mature technique, in which the natural PADM can be well preserved after the removal of cells and cellular components.[36,37] PADM is inexpensive due to the abundance of porcine skin and the simple extraction method. The natural 3D collagen network structure ensures its good ductility and biodegradation properties in biological solutions or in the body. Moreover, a purified porcine skin sheet can be easily stereo-tailored to a certain size and shape for a variety of applications. Therefore, PADM appears to be a very promising candidate for building a bone engineering scaffold as a natural 3D collagen porous matrix.

The assembly method of HAp on the PADM is also very import for obtaining a bioactive scaffold for bone tissue engineering. Biomimetic mineralization is a process by which organisms form minerals in a bioenvironment.[38] Simulated body fluid (SBF) with ion concentrations nearly equal to those of human blood plasma has been proposed by Kokubo with the purpose of identifying a material with *in vivo* bone bioactivity instead of using animal for the experiments.[39] Recently, it has been used as a biomimetic mineralization method to prepare biomaterials.[40–42]

In this article, we proposed a new method including precalcification and biomimetic mineralization to prepare a bone tissue engineering scaffold from porcine skin. Using PADM as a matrix, a two-level porous structure is obtained by assembling HAp on the channel surface. The composite scaffold obtained has high mechanical properties and advantages for the cell attachment. The preparation method is low cost, simple, and controllable, and the obtained composite scaffold is very tough and flexible and can easily be tailored to a certain size and shape without a mold. Therefore, it has great potential application for the mass production of high performance bone scaffolds.

Experimental

The HAp-PADM scaffold was prepared by constructing the HAp nanostructure in channels of PADM framework by a two-step biomimetic mineralization process in SBF.

Preparation of SBF

SBF was prepared in accordance with Kokubo's method.[43] The ion concentrations (mM) are as follows: Na^+ (142), K^+ (5), Mg^{2+} (1.5), Ca^{2+} (2.5), Cl^- (120), HCO_3^- (27), HPO_4^{2-} (2.27), SO_4^{2-} (0.5), NaCl (8.035 g), $NaHCO_3$ (0.355 g), KCl (0.225 g), $K_2HPO_4 \cdot 3H_2O$ (0.231 g), $MgCl_2 \cdot 6H_2O$ (0.311 g), 1M HCL (38 mL), $CaCl_2 \cdot 2H_2O$ (0.3675 g), $NaSO_4 \cdot 10H_2O$ (0.071 g), and $NH_2C(CH_2OH)_3$ (*Tris* buffer, 6.118 g). The reagents were dissolved in the above order into 800 mL of Millipore water at 36.5°C under continuous stirring. Millpore water was added to increase the total volume to 890 mL, the temperature was returned to 36.5°C, and the pH was balanced to 7.4 using 1M HCl. Sodium azide (0.02(wt)%) was added to the SBF to restrain the bacteria. The final volume of the solution was added to 1 L of millipoer water.

All the inorganic reagents are purchased from Sinopharm Chemical Reagent Co., Ltd. Triss Buffer was purchased from Sigma.

Preparation of PADM scaffold

Fresh porcine skin was purchased from a local slaughterhouse. The preparation method of the PADM scaffold is described in our patent (CN03139063.3). Briefly, after complete cleaning, excision of the subdermal fat tissue, and removal of hair, the skin was cut into pieces with a thickness of 1.0 mm and purified through basic processing and enzymatic extraction methods to remove the fat and cells. The product was washed carefully with distilled water, and the moisture-laden purified porcine skin was frozen at −80°C. After lyophilization at −60°C for 4 h, a PADM framework was obtained (Fig. 1a).

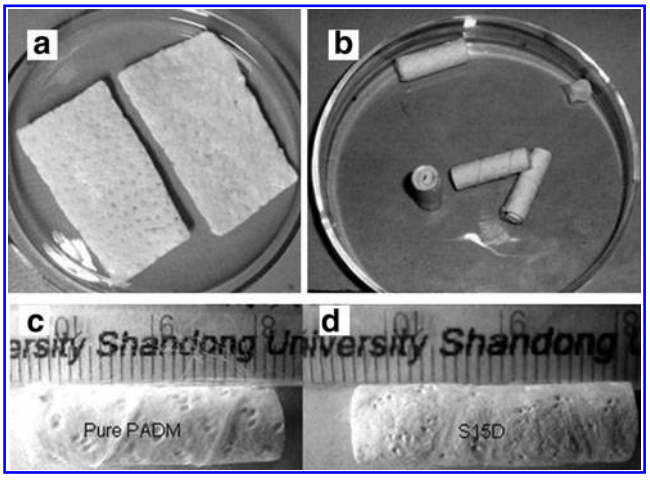

FIG. 1. Photos of the samples. **(a)** The pure PADM sheets. **(b)** The cylinder-shaped samples convolved from PADM sheets. **(c)** Pure PADM cylinder. **(d)** HAp-PADM cylinder (S15D). PADM, porcine acellular dermal matrix; Hap, hydroxyapatite.

Construction of HAp-PADM scaffold

First, PADM framework was cut into 10 mm×10 mm×1 mm flakes. Twenty pieces of the above PADM were pre-calcified through rinsing in 400 mL of 0.1 M $CaCl_2$, K_2HPO_4, and $CaCl_2$ solution for 24 h in an incubation shaker (120 r/min, 37°C) by using an alternative soaking method. Washing with double deionized H_2O (ddH_2O) for 20 min was needed between every two steps to remove the free and weakly connected Ca^{2+} and HPO_4^{2-}. Finally, the Pre-calcification PADM framework was mineralized in 1L SBF in an incubation box at 37°C for 4, 8, 15, and 30 days to obtain HAp-PADM scaffolds. The HAp-PADM scaffolds were washed completely and frozen at −80°C, and freeze-dried at −60°C for 4 h in a vacuum lyophilizer. The samples mineralized for 4, 8, 15, and 30 days were designated as S4D, S8D, S15D, and S30D.

Structural and morphological characterization

X-ray powder diffraction (XRD) data were recorded on a Japan Burker D8/advance X-ray diffractometer system with graphite monochromatized Cu Kα irradiation (λ = 0.15418 nm), together with a diffractometer scan step size of 2θ = 0.02°, and dwell time of 2 s/step, over a 2θ range of 10–70°. Scanning electron microscope (SEM; Hitachi, S-4800) was used to characterize the morphology of the pure PADM and the mineralization process of the HAp on the collagen fibrils at an accelerating voltage of 10 kV.

The mass fraction of HAp in the HAp-PADM scaffold

The mass fraction (MF) of HAp in the composite scaffold was calculated by weighing the mass of PADM framework before and after mineralization in SBF at different time periods. The *MF* was calculated through Equation 1:

$$MF = \frac{m_1 - m_0}{m_1} \times 100\% \quad (1)$$

In the equation, m_1 is the mass of HAp-PADM scaffold after biomimetic mineralization in SBF, whereas m_0 is the mass of pure PADM before biomimetic mineralization in SBF. *MF* is the average value of 15 samples for each composition.

Mechanical properties

To mechanical property measurement, the HAp-PADM scaffolds were first rinsed in phosphate buffered saline (PBS; pH 7.4) for a while and then manually convolved into cylinder-shaped samples measuring 5 mm in diameter and 20 mm in height (Fig. 1c, d). The cylinders were finally frozen at −80°C in an ultra-low temperature refrigerator and then lyophilized at −60°C. Pure PADM and sample S15D were used for the mechanical property measurements. Five specimens were evaluated for each composition. The dry scaffolds were directly used to measure the compressive strength, whereas the wet ones were first rinsed in PBS (pH 7) for 20 min and then tested on the machine. Resistance to mechanical compression of both dry and wet scaffolds was performed on a computer-controlled universal material testing machine (WDW-1, Jinan). The testing process was referred to as Kim's method with 5 mm/min crosshead speed.[44] The elastic modulus (EM) was defined by the slope of the initial linear section of the stress–strain curve. The Young's modulus of each scaffold was determined between strains of 1% and 2.5%.

In vitro *biodegradation rate*

Samples for degradation rate test were cut into small bulks weight about 20 mg for each. Fifteen bulks (pure PADM and S15D) for each composition were first placed in 10 mL of 100 μg/mL collagenase PBS (pH 7.4, 0.01 M; Solarbio). The solution was then incubated at 37°C for 12, 24, 36, 48, 72, and 96 h. The collagenase solution was replaced by a fresh one every 12 h. At the end of each time point, three samples for each composition were removed from the solution, washed with distilled water, and lyophilized. The degradation rate was calculated through Equation 2.

$$DR = \frac{W_0 - W_1}{W_0} \times 100\% \quad (2)$$

where *DR* is the degradation rate, W_0 is the initial dry weight of the samples, and W_t is the dry weight of the scaffold at each time point ($n = 3$).

Cell culture

MC3T3-E1 mouse pre-osteoblast cells (Cell Bank of Chinese Academy of Sciences) were cultured *in vitro* using α-minimal essential medium (MEM) (Gibco) supplemented with 10% fetal bovine serum (FBS; Gibco) and 1% penicillin–streptomycin in a humidified atmosphere of 5% CO_2 at 37°C. For *in vitro* studies, samples were cut into 8 mm×8 mm×0.6 mm plates for cell culture. First, scaffolds were sterilized using 75% ethanol for 2 h in a 24-well culture plate, washed three times in sterile PBS (pH 7.4), and then immersed in α-MEM for 2 h. Finally, scaffolds were seeded with 500 μL of cell suspension containing 50,000 cells. Another 500 μL of fresh culture medium was then added to each scaffold. The culture was maintained for 2 days in an incubator at 37 °C, 5% CO_2, and 95% humidity.

MTT assay

Samples were placed into 24-well plates and seeded with 50,000 cells in 1 mL medium. Proliferation of osteoblast was determined using 3-(4,5-dimethylthiazol-2-yl)-2,5-diphenyltetrazolium bromide (MTT) (Sigma) assay with a time interval of 2, 5, and 7 days. After the prescribed time periods, the specimens were gently rinsed with PBS and transferred to new 24-well plates. Then, 1 ml of the cell culture medium containing 100 μL of MTT solution (5 mg/mL) was added to each well and incubated at 37°C for 4 h to form formazan crystal in cells, which was dissolved by adding 750 μL of dimethyl sulfoxide after the removal of medium. Finally, 250 μL of the MTT solution was transferred to a 96-well plate. The absorbance of each well was measured at 490 nm using a microplate reader.

Confocal laser scanning microscopy observation

Cells after culture for 2 and 7 days on pure PADM framework and S15D scaffold were stained for confocal laser scanning microscope (CLSM) observation. Actin filament was

stained by Alexa-fluor488-phalloidin (green fluorescence; Invitrogen; molecular weight ~1320), which was first dissolved into 1.5 mL methanol to prepare stock solution and the staining procedure was according to the product instruction. However, the concentration of the working solution is thrice higher than that the instruction recommended due to the high adsorption property of PADM scaffold on dye molecules. One milliliter of the concentrated working solution was added to each sample (8 mm×8 mm×0.6 mm). CLSM images were obtained with an Olympus IX71 inverted microscope coupling with a charge-coupled device and a display controller software.

Cell morphology

Cell morphology on the HAp-PADM scaffolds was examined using the (SEM, S-4800) after 48 h of cell seeding. The cell-seeded scaffolds were removed from the culture and gently washed with sterilized PBS. Cells on the scaffolds were fixed with 2.5% glutaraldehyde in PBS for 30 min at 4 °C. After removing the fixative, the scaffolds were subsequently gently washed with PBS and distilled water. These scaffolds were each subjected to sequential dehydration for 10 min with an ethanol series (30%, 50%, 70%, 85%, 90%, 95%, and 100%). After being coated with platinum for 40 s, the scaffolds were allowed to dry for a day and observed under the SEM to assess cell attachment and morphology at a 5 kV accelerating voltage.

Statistical analysis

All data from MTT, degradation rate, and mechanical property results were presented as means ± standard deviation. Statistically significant differences ($p < 0.05$) between the groups were measured by analysis of variance (ANOVA) and Student-Newman-Keuls (SNK) *post hoc* parametric procedure. All statistical analysis was carried out using a SPSS statistical software package (version 13.0).

Results

XRD analysis and MF determination

The phase structure changes of the PADM scaffolds during the mineralization process were determined by X-ray diffraction (Fig. 2). Pure PADM shows a broad peak between 13°–26° caused by the collagen fibrils (Fig. 2a). Figure 2b shows peaks similar to those in Figure 2a, indicating that there is almost no crystalline calcium phosphate or apatite formed on the scaffold after pre-calcification. The inorganic phase can be detected at 2θ value of 31.81° by XRD after biomimetic mineralization in SBF for 4 days (Fig. 2c). The XRD peaks at 2θ values of 25.8°, 31.81°, 32.2°, 39.5°, and 46.8° become stronger with an increase of the mineralization time (Fig. 2d–f), indicating the nucleation and growth of crystals in the PADM framework. The XRD peaks can be indexed based on a hexagonal HAp crystal of space group $P6_3/m$ (a = b = 9.418 Å; c = 6.884 Å) with reference to the standard Powder Diffraction File (card no. 09-432). The broad collagen peak disappears after mineralization in SBF for 15 days (Fig. 2e), because the surface of the collagen fibers is completely coated by thick HAp layers. The XRD pattern of sample S30D is not obviously different from that of sample S15D.

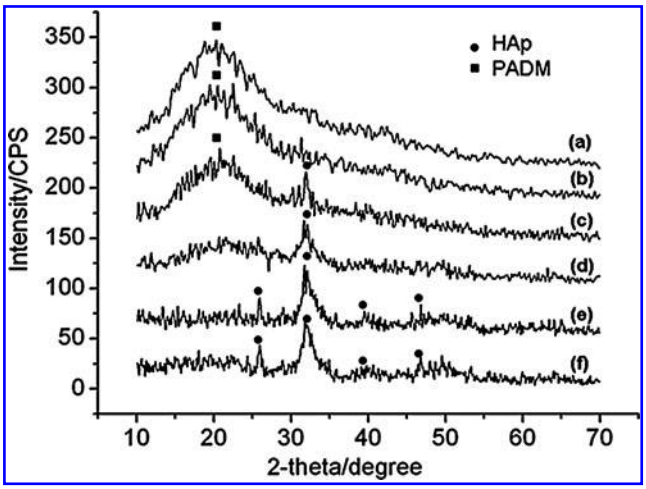

FIG. 2. X-ray diffraction patterns of products. **(a)** Pure PADM. **(b)** Pre-calcification PADM. **(c)** Pre-calcification PADM mineralized in SBF for 4 days (S4D). **(d)** Pre-calcification PADM mineralized in SBF for 8 days (S8D). **(e)** Pre-calcification PADM mineralized in SBF for 15 days (S15D). **(f)** Pre-calcification PADM mineralized in SBF for 30 days (S30D). SBF, simulated body fluid.

It is difficult to assemble HAp on the as-obtained PADM directly in SBF, a pre-calcification process including the sequential immersion of PADM framework in 0.1 M $CaCl_2$, K_2HPO_4, and $CaCl_2$ solution has been designed for the enhancement of mineralization. To explore the effect of pre-calcification on mineralization, control tests were carried out (Fig. 3A). They show that no HAp peaks can be found for PADM without pre-calcification after mineralization in SBF for 4 days (Fig. 3A-a) and only weak crystallite peaks appear for the 24 day sample (Fig. 3A-b). Therefore, the pre-calcification process is necessary to induce the fast formation of HAp on the PADM framework.

Figure 3B shows the average MF variation of HAp in the composite scaffold with mineralization time, reaching 27.2(wt)% for sample S15D and 40.69(wt)% for sample S30D. Here the mass-loss of the PADM caused by degradation in the SBF during the mineralization process is ignored. Therefore, the actual MF of HAp in the scaffold should be slightly higher than the values given in Figure 3B, especially for the samples that were mineralized for 15 and 30 days that had suffered long-term degradation in SBF.

SEM images of the biomimetic mineralization process in SBF

SEM images of pure PADM are shown in Figure 4A. From the low magnification image, we can see that pure PADM is a 3D interconnected network structure. The diameter of the channels is over 100 μm, and the thickness of the channel wall is about 10–20 μm (Fig. 4A-a). The channels are formed from collagen bundles left over after removal of the epidermis, dermal fibroblasts, and epidermal appendages. Multilevel pores co-exist in the large channels (Fig. 4A-b). Figure 4A-c illustrates the morphology of the pore wall and large bundle of collagen fiber. The collagen fibrils are connected with each other along the c-axis. Each fibril has periodic striations, which are spaced ~67 nm apart (Fig. 4A-c). These

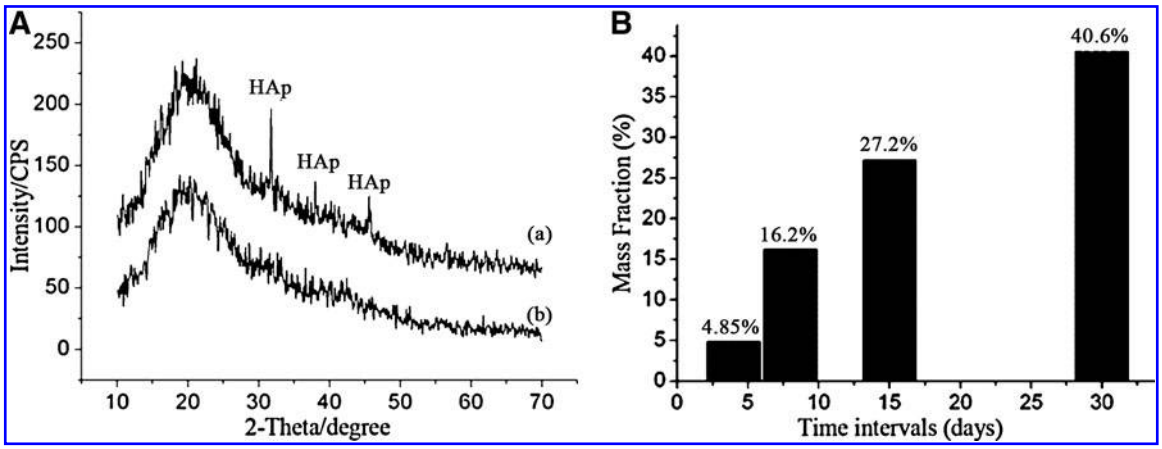

FIG. 3. Control test and the mass fraction (MF) of the samples. **(A)** X-ray diffraction patterns of PADM framework directly biomineralized in SBF without pre-calcification process: **(a)** PADM in SBF for 4 days; **(b)** PADM in SBF for 24 days. **(B)** MFs of HAp in the HAp-PADM scaffold for sample S4D, S8D, S15D, and S30D. The MF is the average value of 15 samples for each composition.

striations are due to the staggering of the tropocollagen, each of which has the complex triple-helix structure.

Figure 4B shows the SEM images of the pre-calcification PADM mineralized in SBF for 4 days (S4D). Compared with pure PADM (Fig. 4A-a), the structure and size of the interconnected channels are well preserved after being mineralized in SBF for 4 days (Fig. 4B-a). Thick pore walls can still be found in large pores (Fig. 4B-b). Figure 4B-c shows that the collagen banding pattern can be identified from the pore wall, but the patterns become vague and some bulges appear on the surface of the channel walls and the bundle of collagen fibrils (Fig. 4B-c, inset). From the XRD results, we conclude that the bulges are the nuclei of HAp, which will eventually grow to be HAp nanocrystals.

Figure 4C shows the images of sample S8D. In Figure 4C-a, the interconnected channels are still preserved after 8 day mineralization in SBF and the structure of a single channel still retains its original shape. A large number of flower-like clusters can be found on the channel wall (Fig. 4C-b, inset). The flower-like HAp consists of small HAp petals $\sim$5 nm in thickness and 100–200 nm in width. The flower-like HAp nanostructures can also be observed on a single collagen fiber (Fig. 4C-c). We infer that the nucleation and growth process of the HAp nanosturctures on the collagen fibrils and walls are similar.

Figure 4D shows the SEM images of sample S15D. The PADM still retains the porous network structure. However, the diameter of the channel is decreased and almost all of the channels are measured to be $<$150 μm (Fig. 4D-a). After 15 day mineralization, the flower-like HAp clusters observed in sample S8D have been replaced by a layer of porous self-assembled 3D continuous network-like nanostructures of HAp (Fig. 4D-b, inset). The micropores are formed by the bending of the HAp flakes sized at 50–120 nm in diameter (Fig. 4D-b inset). Therefore, a 3D two-level porous HAp-PADM scaffold has been formed, which is composed of large channels formed by collagen bundles and nanopores formed by network-like HAp nanostructures. The network-like HAp nanostructures can also be observed on a single collagen fibril in the collagen scaffold (Fig. 4D-c). This kind of flower-like morphology of the clusters is very typical of HAp grown in SBF on many substrates, such as on titanium substrate, Gelatin scaffold.[45,46] Here, we grow them on the channel wall of 3D PADM framework.

Figure 4E illustrates the pre-calcification sample after 30 day mineralization (S30D). Although the PADM maintains the original porous structure (Fig. 4E-a), the interconnected channels cannot be obviously discerned and most of the channels are measured to be $<$100 μm in diameter, which is smaller than those of the short-term mineralized samples. The HAp layer on the channel wall is much thicker than those on the previous samples, and some channels are nearly blocked. A large amount of very thin needle-like HAp particles stand up on the channel wall pointing toward the center of the channel, resulting in a reduction in the channel diameter (Fig. 4E-b, inset). On the surface of the individual collagen fibrils, there are some needle-like HAp nanocrystals growing outward (Fig. 4E-c, inset). The HAp network on the surface of the channel that appeared in sample S15D is replaced by some individual dendrites built up with tiny needle-like HAp nanocrystals.

For bone tissue engineering applications, the interconnected pore diameter of scaffolds should be about 100 μm for nutrition supply and bone formation.[47,48] The overgrowth of the crystals on PADM in SBF brings about an irregular and thick HAp layer on the channel surface of sample S30D, which decreases the diameter of interconnected pores and is not beneficial for cell migration, while sample S8D has low HAp content resulting in low mechanical strength. Therefore, sample S15D is selected for cell culture and biological tests in the next phase of our work on account of its 3D two-level porous structure and pure PADM as a control due to its excellent bioactivity in skin tissue engineering.

Mechanical and in vitro *biodegradation properties*

Compression testing reveals a different stress–strain behavior for dry PADM and sample S15D, and wet sample S15D. The EM of dry sample S15D is 145 MPa, which is much

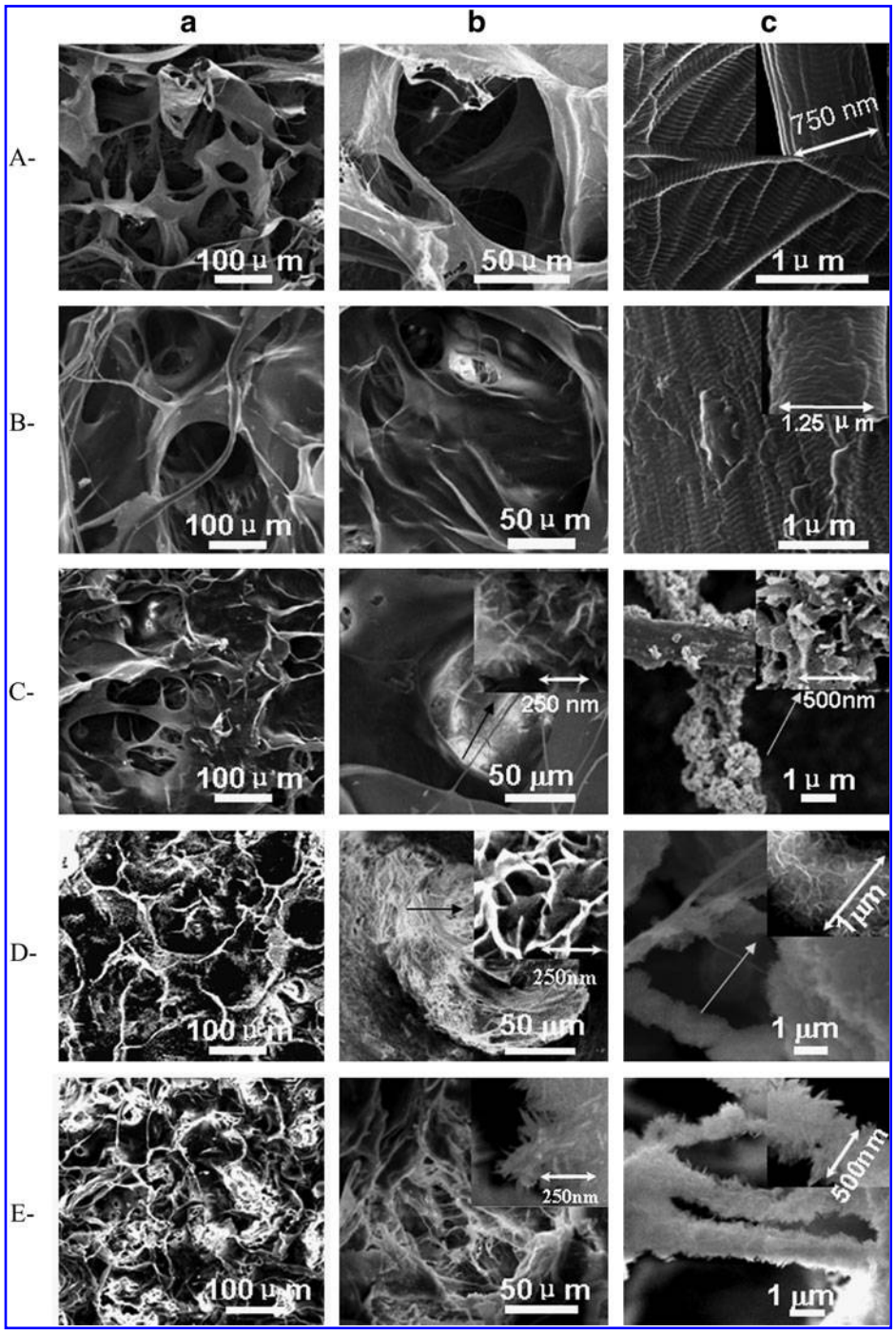

FIG. 4. Scanning electron microscopy (SEM) images of pure PADM framework **(A-a, b, c)**, sample S4D **(B-a, b, c)**, sample S8D **(C-a, b, c)**, sample S15D **(D-a, b, c)**, and sample S30D **(E-a, b, c)**. Column **(a)**: The interconnected channels. Column **(b)**: The typical morphology of a single channel. Column **(c)**: Higher magnification view of the channel wall or one collagen bundle. The local magnifications of insets are denoted by arrows.

higher than that of dry pure PADM with an EM value of 40 MPa (Fig. 5A), indicating that the assembly of HAp can obviously reinforce the PADM scaffold. PADM is extracted from fresh porcine skin, which is soft tissue and cannot bear high load in moisture. Therefore, the compressive EM value of pure PADM scaffold in wet condition cannot be measured. However, it shows relatively high compressive EM value of 600 kPa after the incorporation of HAp (Fig. 5A, inset).

Figure 5B displays the biodegradation rate of the samples in collagenase solution at 37°C. On the whole, the weight loss for all the samples reveals an ascending trend with the increasing time. After 12 h of degradation, there are no significant difference between pure PADM and S15D ($p = 0.324$). As for pure PADM, the increase of degradation rate can be discerned obviously after 36 h, whereas S15D has a significant increase at 72 h. It can be found that the degradation rate of pure PADM reaches as high as 98% at 72 h, which is much higher than that of 39% for sample S15D ($p < 0.01$). After 96 h in collagenase solution, the pure PADM can be completely degraded and the weight loss of S15D reaches as high as 58%. The assembly of HAp effectively influences on the biodegradable property of collagen.

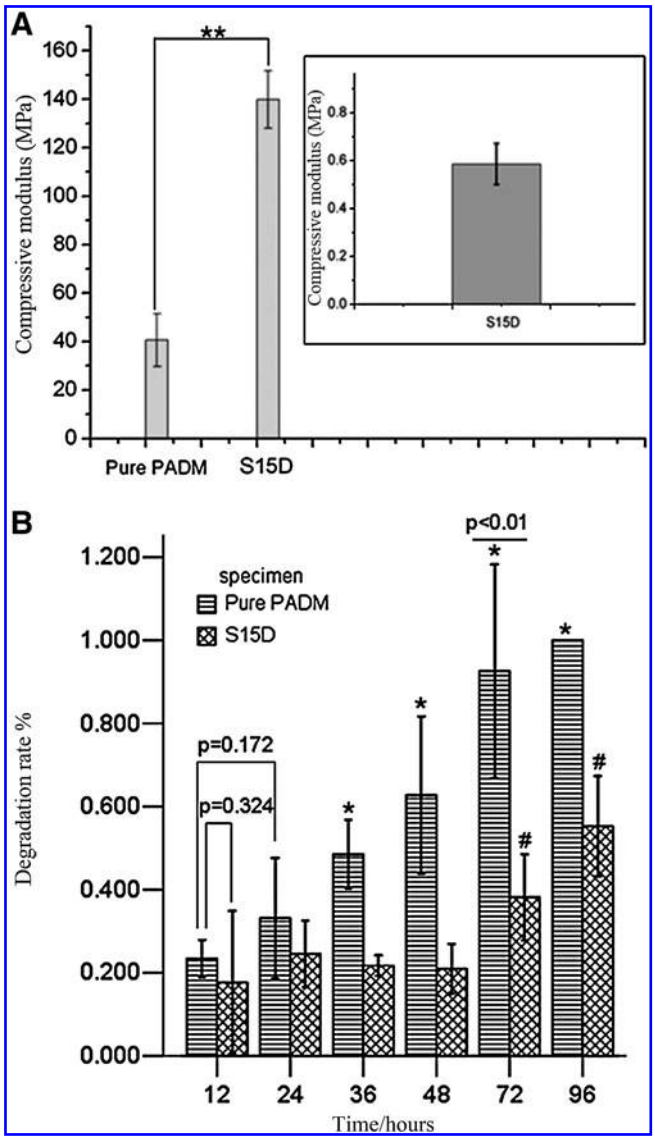

FIG. 5. Mechanical and *in vitro* biodegradation properties of the samples. **(A)** Compressive elastic modulus of dry PADM, HAp-PADM scaffold mineralized for 15 days (S15D), and wet HAp-PADM scaffold (S15D) (inset). $^{**}p < 0.05$ represents a statistically significant difference between pure PADM and S15D. Error bars designate SD ($n = 5$). **(B)** *In vitro* degradation rate of pure PADM and S15D at different time points. Symbols (*, #) represent a statistically significant difference as compared with the degradation rate of 12 h for each composition ($p < 0.05$). $p = (0.324,\ 0.172)$ represents no statistically significant difference between the two samples. $p < 0.01$ represents a statistically significant difference between pure PADM and S15D at 72 h. Error bars designate SD ($n = 3$). SD, standard deviation.

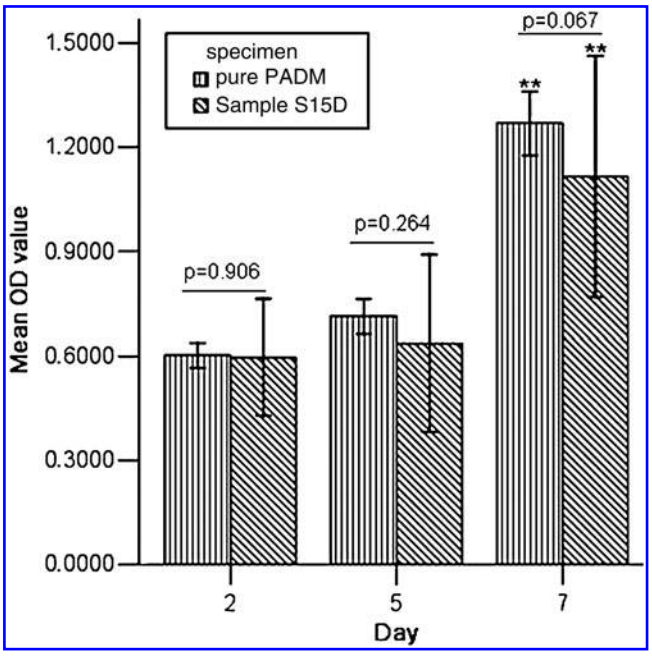

FIG. 6. Cell proliferation on pure PADM framework and sample S15D scaffold after 2, 5, and 7 days. $^{**}p < 0.05$ represents a statistically significant difference as compared with the optical density (OD) value of 2 and 5 days. p (0.906, 0.264, and 0.067) > 0.05 means no statistically significant differences between pure PADM framework and sample S15D at each time point. Error bars designate SD ($n = 5$).

MTT test and CLSM observation

Cell attachment, proliferation, and morphology studies were conducted using MC3T3-E1 pre-osteoblast cells, which have been extensively characterized for their osteogenic differentiation potential.[49,50] MTT has been widely accepted as a characterization method for the cell attachment and proliferation. In the MTT test (Fig. 6), there is no statistically significant difference between pure PADM framework and sample S15D scaffold at each time point during cell culture (p [(0.906, 0.264, and 0.067] > 0.05). No obvious proliferation of pre-osteoblasts can be observed on the two scaffolds after seeding for 5 days. At 7th day after seeding, the optical density (OD) value of cells cultured on pure PADM is at 1.26, while on sample S15D is at 1.0. Compared with the OD value of 2 and 5 days, proliferation of pre-osteoblasts on the two samples can be observed after 7 day culture ($p < 0.05$).

Figure 7 shows the cell morphology and distribution on the scaffold after 2 and 7 day culture. Actin filament was stained by Alexa-fluor488-phalloidin, which could emit green fluorescence when excited by light with a wavelength of 488 nm. Figure 7a shows the cell morphology and distribution of viable cells on pure PADM framework after 2 day culture. It can be observed that cells are distributed on the framework with no ordered arrangement due to the naturally original channels of the PADM framework. Porous surface structure determines the cell position on the scaffold and cause different fluorescence intensity of cells or different part of one cell in and out of focus. Cells cannot spread well on pure PADM after 2 days. After culture for 7 days (Fig. 7b), the cell density appears to be increased, and cells completely spread on the scaffold to be fibroblastic structure. Similar results can be obtained on sample S15D (Fig. 7c, d).

Cell attachment on HAp-PADM scaffold

SEM images show the attachment of MC3T3-E1 cells on the HAp-PADM scaffold after 2 day culture (Fig. 8). Figure 8a shows an image of a cell colony in a channel of the

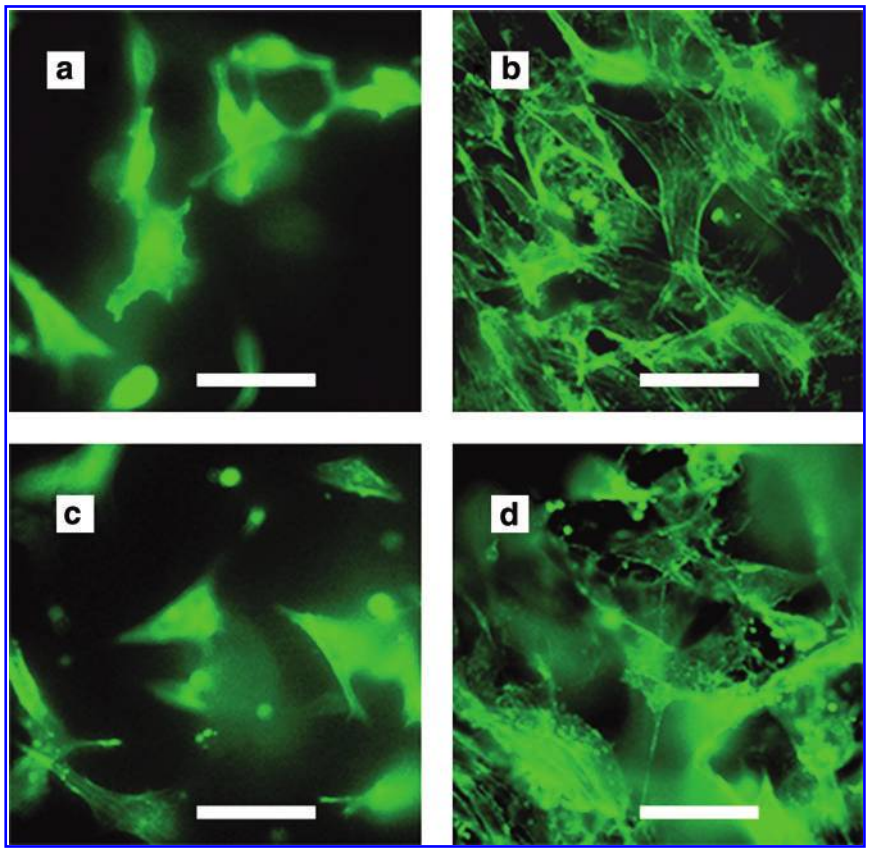

FIG. 7. Confocal laser scanning microscopy (CLSM) images of cell distribution on pure PADM framework **(a, b)** and sample S15D scaffold **(c, d)** after 2 and 7 day culture. Actin filament of the cells was stained with Alexa-fluor488-phalloidin with an excitation wavelength at 488 nm. Bar: 50 μm. Color images available online at www.liebertonline.com/ten.

scaffold. One can observe three cells overlapped together, designated as 1, 2, and 3 (Fig. 8a). With higher magnification, the intimate contact between the cells and materials is evident (Fig. 8b). Figure 8c shows the higher magnification view of the cell filopodia, which intimately adheres to the ECM. In Figure 8d, the ECM directly contacts with the cells in the network-like HAp nanostructure with nanopores sized at about 100 nm as described in Figure 4D.

Discussion

To avoid cross-linking during the construction of porous HAp-collagen scaffold, we chose natural PADM framework as collagen matrix to prepare HAp-PADM bone tissue engineering scaffold. PADM was obtained from porcine skin by a nondestructive extraction process. Therefore, the natural cross-linkage between collagen fibrils was well preserved after the removal of cells and fats, which contributed to the interconnected porous structure and the high tensile strength of PADM framework. The thickness of PADM sheet after extraction treatment is almost the same as raw skin measured at 1 mm in thickness. Due to the soft tissue origin and the direct utility of bulk PADM framework, it is very difficult to assemble nano-HAp particles in the 3D PADM framework uniformly by using traditional co-precipitation method, whereas one-step biomimetic mineralization method takes so long time for HAp fabrication on PADM. Therefore, a two-step biomimetic mineralization process, including precalcification and biomimetic mineralization in SBF, was developed for the preparation of HAp-PADM scaffold. This two-step biomimetic mineralization method ensures the uniform heterogeneous nucleation and growth of HAp nanostructure on natural 3D PADM framework.

Continual XRD and SEM characterization were employed to observe the phase composition and morphology changes in the scaffold at different time points during biomimetic mineralization process (Figs. 2–4). It has been reported that materials with repetitive patterns of anionic groups trap inorganic cations, leading to the nucleation and growth of oriented crystals *in vivo*.[51] Large amounts of amino acid residues remain on the surface of the collagen fibrils,[52] which can form polar ionic clusters that are highly electriferous, and help gather inorganic ions onto the active sites of the collagen surface. After 15 day mineralization in SBF, a layer of nano-HAp porous structure was formed on the channel wall of PADM framework (Fig. 4D), and the interconnected channels of PADM were still maintained after the long time biomimetic mineralization process. Therefore, HAp-PADM scaffold with two-level pores is formed, which can be schematically described as shown in Figure 9. Sample S15D is chosen as scaffold in the degradation and mechanical property tests, and cell culture experiments due to its high content of HAp and proper two-level interconnected porous structure.

Scaffold material is one of the basic factors for tissue engineering. The degradation property of scaffold material is very important. In our experiments, it is proved that envelop of HAp layer on collagen fibers can influence on the *in vitro* degradation rate of collagen in collagenase solution (Fig. 5B). Pure PADM shows a time-dependent increase of degraded matrix in the presence of collagenase. In contrast, the S15D matrix shows essentially a constant degradation until 72 h. It

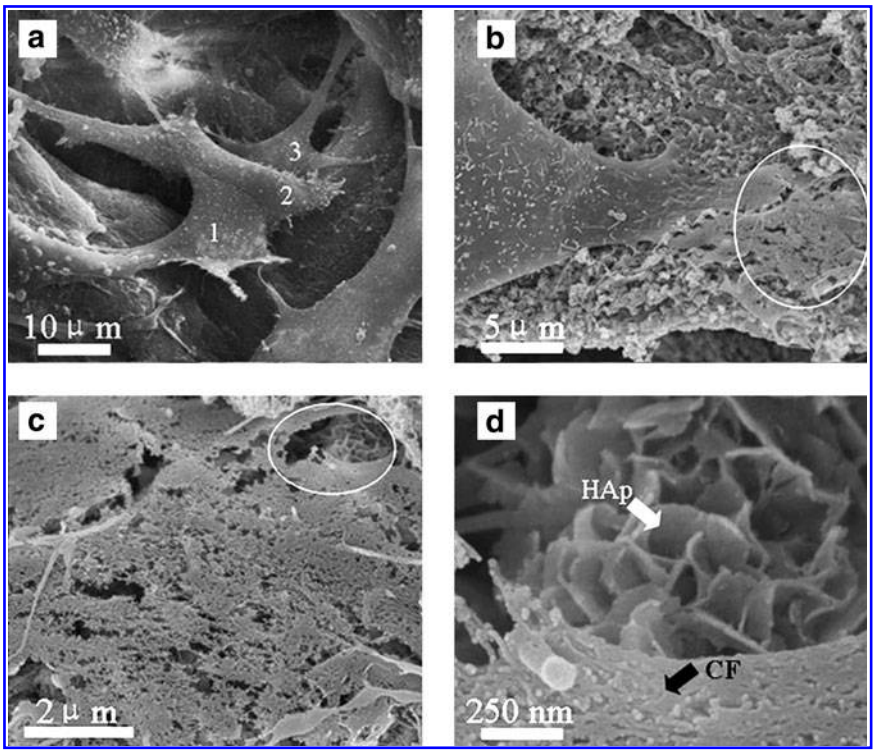

FIG. 8. SEM images of MC3T3-E1cells on HAp-PADM scaffold. **(a)** Cells observed in the channel. Arabic numbers 1, 2, and 3 mark three cells that spread over the channel. **(b)** Higher magnification view of one cell. **(c)** Magnification of the circled part of image **(b)**. **(d)** Magnification of the circled part of image **(c)**. White arrow designates the network-like HAp nanostructure, and black arrow designates the cell filopodia (CF).

is possible that the S15D has, at that time, lost enough of the protective HAp coating that it is susceptible to proteolysis after 72 h (Fig. 5 B). It suggests that the degradation rate of HAp-PADM scaffold can be controlled by changing the biomimetic mineralization time in SBF.

A basic requirement for a scaffold is that the scaffold should be mechanically strong for the cell in-growth and matrix production until tissue regeneration. PADM has high tensile strength, while their compressive strength is very low. In our experiments, it shows relatively high compressive EM value of 600 kPa after the incorporation of HAp, which is much higher than the value of 1 and 95 kPa of HAp-collagen scaffold recently reported by the similar method.[53,54] Infiltration of HAp among the collagen fibrils plays an important role in reinforcing the PADM framework. On one hand, the natural PADM that formed a soft framework structure can contribute to the toughness and ductility of the scaffold, that is, its ability to undergo deformation and absorb energy after it begins to yield to soft tissues.[55,56] On the other hand, HAp as the mineral phase that inserts into and envelops the PADM increases the stiffness of the scaffold. Therefore, the HAp-PADM scaffold prepared with this method has both the tensile strength from PADM and the compressive resistance that may better meet the requirements for bone substitute materials. Moreover, PADM has a long history of use in skin tissue engineering,[7,34,35] whereas HAp is the main component of bone, indicating that both of them have good biocompatibility.

MC3T3-E1 preosteoblasts have been widely used as model cell to investigate various cell behaviors on scaffolds for the application of both dental implants and bone substitute materials.[57,58] In this study, they were employed to characterize the cell morphology and *in vitro* cell proliferation on HAp-PADM composite scaffold material. MTT is a traditional method in cytotoxicity test of scaffold and CLSM has been widely used for the cell morphology and distribution observation. In our study, both MTT and CLSM results indicate that there are no statistically significant difference between HAp-PADM scaffold and PADM framework for the culture of pre-osteoblasts at different time points.

MTT results show that cell proliferation on pure PADM can be observed after 5 days, whereas no proliferation can

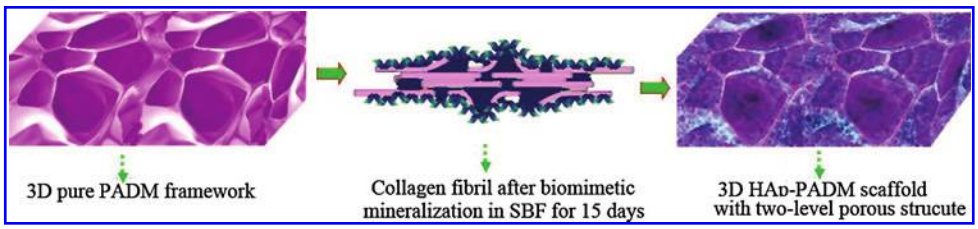

FIG. 9. Schematic description of pure PADM framework and the two-level porous HAp-PADM scaffold. Color images available online at www.liebertonline.com/ten.

be observed on sample S15D. Proliferation on both pure PADM and S15D can be observed at 7th day. That is because the prepared scaffolds are highly porous with high water uptaking property. FBS in the culture medium can be easily immersed into the scaffolds and adsorbed by the hydroxyl groups and amino acid residues of collagen, resulting in the lack of FBS in the culture medium to maintain the normal cell proliferation. However, although a large amount of FBS is adsorbed into scaffolds, cells on the scaffold can still live on the FBS adsorbed on the scaffold surface and in the culture medium but their growth is obviously restrained. The culture medium with FBS is changed every 2 days for MTT assay. The protein adsorption will be saturated on the scaffold surface after twice changes. If given enough FBS adsorption on the scaffolds, cell proliferation on the scaffolds can be observed at 5th day (see Supplementary Fig. S1; Supplementary Data are available online at www.liebertonline.com/ten). Therefore, proliferation on both pure PADM and sample S15D can be observed at 7th day. CLSM results support this point, which give the expected results of cell distribution and spread on the scaffolds. The exact interaction between cells and HAp-PADM matrix is characterized by SEM, which have higher magnification and resolving power. It shows that cell filopodia can tightly adhere to secondary nanoporous structure formed by flake-like HAp. It has been reported that most of the ECM are nanoscale in dimension and they play an important role in stimulating cell growth, and thus guide tissue regeneration.[59] Here the obtained HAp-PADM scaffold has a two-level porous structure, with large channels ($\sim$100 μm in diameter) inherited from the purified PADM microstructure, and small pores (<100 nm in diameter) made up of self-assembled HAp on the channel surfaces. The former benefits the transportation of nutrients and metabolic wastes and the cell migration in the scaffold. The latter are beneficial not only for the degradation of collagen and absorption of HAp, but also for the attachment and growth of cells in a plasma environment.

Conclusions

We have demonstrated the fabrication of a HAp-PADM scaffold with a 3D two-level porous structure by assembling the HAp nanostructures on the channel surface of PADM framework using a two-step biomimetic mineralization method. The HAp-PADM scaffold mineralized in SBF for 15 days has both interconnected channels ($\sim$100 μm in diameter) formed by collagen fiber bundles and nanopores (<100 nm in diameter) self-assembled by HAp flakes. The pre-calicification process plays an important role in promoting the formation of HAp nuclei on the PADM, and the biomimetic mineralization process in SBF contributes to the formation of HAp nanostructures. The compressive EM value of wet sample S15D is as high as 600 kPa, and CLSM and MTT results show similar morphology and proliferation of MC3T3-E1 cells on pure PADM framework and S15D scaffold, indicating that the S15D has relatively high mechanical strength but no cytotoxicity *in vitro*. It can be concluded that HAp-PADM scaffold is a promising scaffold for bone repair and our method indicates that natural ADM as a soft tissue base has potential use in bone tissue engineering.

Acknowledgments

This research was supported by NSFC (NSFDYS: 50925205; Grant: 50990303, 50872070; IRG: 50721002), the Major State Basic Research Development Program of China (2010CB833103). Independent Innovation Foundation of Shandong University (2009JC011), and the Program of Introducing Talents of Discipline to Universities in China (111 program no. b06015).

Disclosure Statement

No competing financial interests exist.

References

1. American Academy of Orthopedic Surgeons (AAOS), online: www.aaos.org/Research/stats/patientstats.asp.
2. Langer, R., and Vacanti, J.P. Tissue engineering. Science **260,** 920, 1993.
3. Moutos, F.T., Freed, L.E., and Guilak, F.A. Biomimetic three-dimensional woven composite scaffold for functional tissue engineering of cartilage. Nat Mater **6,** 162, 2007.
4. Liu, X.H., Smith, L.A., Hu, J., and Peter, X.M. Biomimetic nanofibrous gelatin/apatite composite scaffolds for bone TE. Biomaterials **30,** 2252, 2009.
5. Wu, S.L., Liu, X.M.T., Hu, P.K., Chu, J.P.Y., Ho, Y.L., Chan, K.W.K., Yeung, C.L., Chu, T.F., Hung, K.F., Huo, C.Y., Chung, W.W., Lu, K.M.C., and Cheung, K.D.K. A biomimetic hierarchical scaffold: natural growth of nanotitanates on three-dimensional microporous ti-based metals. Nano Letters **11,** 3083, 2008.
6. Turek, S.L. Orthopaedics: Principles and Their Application, 2nd edition. Philadelphia: Lippincott Williams & Wilkins, 1985, p. 113.
7. Heitland, A., Piatkowski, A., Noah, M.E., and Pallua, N. Update on the use of collagen/glycosaminoglycate skin substitute—six years of experiences with artificial skin in 15 German burn centers. Burns **30,** 471, 2004.
8. Still, J., Glat, P., Silverstein, P., Griswold, J., and Mozingo, D. The use of a collagen sponge/living cell composite material to treat donor sites in burn patients. Burns **29,** 837, 2003.
9. Anselme, K. Osteoblast attachment on biomaterials. Biomaterials **21,** 667, 2000.
10. Kleinman, H.K., Klebe, R.J., and Martin, G.R. 1981 Role of collagenous matrices in the attachment and growth of cells. J Cell Biol **88,** 473, 2000.
11. Morra, M., Cassinelli, C., Cascardo, G., Cahalan, P., Cahalan, L., Fini, M., and Giardino, R. Surface engineering of titanium by collagen immobilization. Surface characterization and *in vitro* and in vivo studies.Biomaterials **24,** 4639, 2003.
12. Lee, C.H., Singla, A., and Lee, Y. Biomedical applications of collagen. Int J Pharm **221,** 1, 2001.
13. Kikuchi, M., Itoh, S., Ichinose, S., Shinomiya, K., and Tanaka, J. Self-organization mechanism in a bone-like hydroxyapatite/collagen nanocomposite synthesized *in vitro* and its biological reaction *in vivo*. Biomaterials **22,** 1705, 2001.
14. Chang, M.C., Ikoma, T., Kikuchi, M., and Tanaka, J. Preparation of a porous hydroxyapatite/collagen nanocomposite using glutaraldehyde as a crosslinking agent. J Mater Sci Lett **20,** 1199, 2001.
15. Yap, A.U.J., Pek, Y.S., Kumar, R.A., Cheang, P., and Khor, K.A. Experimental studies on a new bioactive material: HAp-ionomer cements. Biomaterials **23,** 955, 2002.
16. Gosain, A.K., Song, L., Riordan, P., Amarante, M.T., Nagy, P.G., and Wilson, C.R. A 1-year study of osteoinduction in

hydroxyapatite-derived biomaterials in an adult sheep model: part I. Plast Reconstr Surg **109,** 619, 2002.
17. Lin, L., Chow, K.L., and Leng, Y. Study of hydroxyapatite osteoinductivity with an osteogenic differentiation of mesenchymal stem cells. J Biomed Mater Res A **89,** 326, 2009.
18. Jiao, Y.P., Liu, Z.H., and Zhou, C.R. Fabrication and characterization of PLLA–chitosan hybrid scaffolds with improved cell compatibility. J Biomed Mater Res A **80,** 820, 2007.
19. Kim, I.Y., Seo, S.J., Moon, H.S., Yoo, M.K., Park, I.Y., Kim, B.C., and Cho, C.S. Chitosan and its derivatives for TE applications. Biotechnology Advances **26,** 1, 2008.
20. Zhao, F., Grayson, W.L., Ma, T., Bunnell, B., and Lu, W.W. Effects of hydroxyapatite in 3-D chitosan–gelatin polymer network on human mesenchymal stem cell construct development. Biomaterials **27,** 1859, 2006.
21. Du, C., Cui, F.Z., Feng, Q.L., Zhu, X.D., and de Groot, K. Tissue response to nano-hydroxyapatite/collagen composite implants in marrow cavity. J Biomed Mater Res **42,** 540, 1998.
22. Liu, C.Z. Biomimetic synthesis of collagen/nano-hydroxyapitate scaffold for TE. J Bionic Eng Suppl **5,** 1, 2008.
23. Lickorish, D., Ramshaw, J.A.M., Werkmeister, J.A., Glattauer, V., and Howlett, C.R. Collagen–hydroxyapatite composite prepared by biomimetic process. J Biomed Mater Res A **68,** 19, 2004.
24. Tsai, S.W., Hsu, F.Y., and Chen, P.L. Beads of collagen–nanohydroxyapatite composites prepared by a biomimetic process and the effects of their surface texture on cellular behavior in MG63 osteoblast-like cells. Acta Biomaterialia **4,** 1332, 2008.
25. Zhao, H.G., Ma, L., Gao, C.Y., and Shen, J.C. Fabrication and properties of mineralized collagen-chitosan/hydroxyapatite scaffolds.Polym Adv Technol **19,** 1590, 2008.
26. Zhang, W., Liao, S.S., and Cui, F.Z. Hierarchical self-assembly of nano-fibrils in mineralized collagen. Chem Mater **15,** 3221, 2003.
27. Bigi, A., Cojazzi, G., Panzavolta, S., Rubini, K., and Roveri, N. Mechanical and thermal properties of gelatin films at different degrees of glutaraldehyde crosslinking. Biomaterials **22,** 763, 2001.
28. Khor, E. Methods for the treatment of collagenous tissues for bioprostheses. Biomaterials **18,** 95, 1997.
29. Matsuda, S., Iwata, H., Se, N., and Ikada, Y. Bioadhesion of gelatin films cross-linked with glutaraldehyde. J Biomed Mater Res **45,** 20, 1999.
30. Ge, L.P., Zheng, S.Q., and Wei, H. Comparison of histological structure and biocompatibility between human acellular dermal matrix (ADM) and porcine ADM. Burns **35,** 46, 2009.
31. Ng, K.W., Khor, H.L., and Hutmacher, D.W. *In vitro* characterization of natural and synthetic dermal matrices cultured with human dermal fibroblasts. Biomaterials **25,** 2807, 2004.
32. Chai, J.K., Liang, L.M., Yang, H.M., Feng, R., Yin, H.N., Li, F.Y., and Sheng, Z.Y. Preparation of laser micropore porcine acellular dermalmatrix for skin graft: an experimental study. Burns **33,** 719, 2007.
33. Takami, Y., Matsuda, T., Yoshitake, M., Hanumadass, M., and Walter, R.J. Dispase/detergent treated dermal matrix as a dermal substitute. Burns **22,** 182, 1996.
34. Takami, Y., Matsuda, T., Yoshitake, M., Hanumadass, M., and Walter, R.J. Dispase/detergent treated dermal matrix as a dermal substitute. Burns **21,** 243, 1995.
35. Chai, J.K., Liu, Q., and Feng, R.A. Comparative study on transplantation of xenogeneic (porcine) acellular dermal matrix combined with micro-autograft or split-thickness autograft of skin. Med J Chin PLA **29,** 714, 2004.
36. Chen, R.N., Ho, H.O., Tsai, Y.T., and Sheu, M.T. Process development of an acellular dermal matrix (ADM) for biomedical applications. Biomaterials **25,** 2679, 2004.
37. Lee, Y., Chen, M.Y., Kuo, C.Y., and Chang, H.C. Preparation of porcine dermal matrix graft. Taibei: Global Chinese Symposium on Biomaterials and Controlled Release **13,** 584, 1999.
38. Lowenstam, H.A. Minerals formed by organisms. Science **211,** 1126, 1981.
39. Kokubo, T. Bioactive glass ceramics: properties and applications. Biomaterials **12,** 155, 1991.
40. Takadama, H., Kim, H.M., Kokubo, T., and Nakamura, T. TEM-EDX study of mechanism of bonelike apatite formation on bioactive titanium metal in simulated body fluid. J Biomed Mater Res **57,** 441, 2001.
41. Nishiguchi, S., Fujibayashi, S., Kim, H.M., Kokubo, T., and Nakamura, T. Biology of alkali- and heat-treated titanium implants. J Biomed Mater Res **67A,** 28, 2003.
42. Juhasz, J.A., Best, S.M., Auffret, A.D., and Bonfield, W. Biological control of apatite growth in simulated body fluid and human blood serum. J Mater Sci Mater Med **19,** 1823, 2008.
43. Kokubo, T., and Takadama, H. How useful is SBF in prediction in vivo bone bioactivity? Biomaterials **27,** 2907, 2006.
44. Landis, W.J., Hodgens, K.J., Song, M.J., Arena, J., Kiyonaga, S., Marko, M., Owen, C., and McEwen, B.F. Mineralization of collagen may occur on fibril surfaces: evidence from conventional and high-voltage electron microscopy and three-dimensional imaging. J Struct Biol **117,** 24, 1996.
45. Wang, X.J., Li, Y.C., Lin, J.G., Hodgson, P.D., and Wen, C. Effect of heat-treatment atmosphere on the bond strength of apatite layer on Ti substrate. Dental Materials **24,** 154, 2008.
46. Liu, X.H., Smith, L.A., Hu, J., and Ma, P.X. Biomimetic nanofibrous gelatin/apatite composite scaffolds for bone tissue engineering. Biomaterials **30,** 225, 2009.
47. Hofmann, S., Hagenmüller, H., Koch, A.M., Müller, R., Vunjak-Novakovic, G., Kaplan, D.L., Merkle, H.P., and Meinel, L. Control of *in vitro* tissue-engineered bone-like structures using human mesenchymal stem cells and porous silk scaffolds. Biomaterials **28,** 1152, 2007.
48. Kong, L., Ao, Q., Wang, A., Gong, K., Wang, X., Lu, G., Gong, Y., Zhao, N., and Zhang, X. Preparation and characterization of a multilayer biomimetic scaffold for bone tissue engineering. J Biomater Appl **22,** 223, 2007.
49. Jackson, R.A., Murali, S., van-Wijnen, A.J., Stein, G.S., Nurcombe, V., and Cool, S.M. Heparan sulfate regulates the anabolic activity of MC3T3-E1 preosteoblast cells by induction of Runx2. J Cell Physiol **210,** 38, 2007.
50. Kong, H.J., Boontheekul, T., and Mooney, D.J. Quantifying the relation between adhesion ligand–receptor bond formation and cell phenotype. Proc Natl Acad Sci **103,** 18534, 2006.
51. Hartgerink, J.D., Beniash, E., and Stupp, S.I. Self-assembly and mineralization of peptide-amphiphile nanofibers. Science **294,** 1684, 2001.
52. Cowin, S.C. Do liquid crystal-like flow processes occur in the supramolecular assembly of biological tissues? J Non-Newtonian Fluid Mec **119,** 155, 2004.
53. Al-Munajjed, A.A., Plunkett, N.A., Gleeson, J.P., Weber, T., Christian, J., Levingstone, T., Hammer, J., and O'Brien, F.J.

Development of a biomimetic collagen-hydroxyapatite scaffold for bone engineering using a SBF immersion technique. J Biomed Mater Res Part B Appl Biomater **90B,** 584, 2009.
54. Al-Munajjed, A.A., and O'Brien, F.J. Influence of a novel calcium-phosphate coating on the mechanical properties of highly porous collagen scaffold for bone repair. J Mech Behav Biomed **2,** 138, 2009.
55. Burr, D.B. The contribution of the organic matrix to bone's material properties. Bone **31,** 8, 2002.
56. Currey, J.D. Role of collagen and other organics in the mechanical properties of bone. Osteoporos Int **14,** 29, 2003.
57. Yang, X.F., Chen, Y., Yang, F., He, F.M., and Zhao, S.F. Enhanced initial adhesion of osteoblast-like cells on an anatase-structured titania surface formed by H_2O_2/HCl solution and heat treatment. Dental Materials **25,** 473, 2009.
58. Liu, X.H., Smith, L.A., Hu, J., and Ma, P.X. Biomimetic nanofibrous gelatin/apatite composite scaffolds for bone tissue engineering. Biomaterials **30,** 2252, 2009.
59. Zhang, L.J., and Webster, T. Nanotechnology and nanomaterials: promises for improved tissue regeneration. J Nano Today **4,** 66, 2009.

Address correspondence to:
Hong Liu, Ph.D.
State Key Laboratory of Crystal Materials
Center of Bio and Micro/Nano Functional Materials
School of Physics and Microelectronics
Shandong University
27 Shanda Nanlu
Jinan 250100
P.R.China

E-mail: hongliu@sdu.edu.cn

Received: March 29, 2010
Accepted: October 21, 2010
Online Publication Date: December 3, 2010